Chemical Effect of Hydrodynamic Cavitation: Simulation and Experimental Comparison

Mauro Capocelli and Dino Musmarra
Dept. di Ingegneria Civile, Design, Edilizia e Ambiente, Seconda Università degli Studi di Napoli, Aversa (CE) 81031, Italy

Marina Prisciandaro
Dept. di Ingegneria Industriale, dell'Informazione e di Economia, Università dell'Aquila, L'Aquila 67100, Italy

Amedeo Lancia
Dept. di Ingegneria Chimica, dei Materiali e della Produzione Industriale, Università "Federico II" di Napoli, Napoli 80125, Italy

DOI 10.1002/aic.14472
Published online May 5, 2014 in Wiley Online Library (wileyonlinelibrary.com)

The chemical effect of hydrodynamic cavitation (HC) in a Venturi reactor from both the theoretical and the experimental point of view is dealt. A mathematical model is presented to simulate the global production of hydroxyl radicals; it is based on a set of ordinary differential equations that account for the hydrodynamics, mass diffusion, heat exchange, and chemical reactions inside the bubbles. Experimentally, the degradation of p-nitrophenol (initial concentration 0.15 g dm^{-3}) has been conducted in a lab scale Venturi reactor at inlet pressure ranging from 0.2 to 0.6 MPa and has been used to estimate the hydroxyl radical production. The optimum configuration, suggested by numerical simulations, has been experimentally confirmed. Thanks to the empirical validation, this novel modeling approach can be considered as a theoretical tool to identify the best configuration of HC operating parameters. © 2014 American Institute of Chemical Engineers *AIChE J*, 60: 2566–2572, 2014

Keywords: bubble dynamics, hydrodynamic cavitation, numerical modeling, hydroxyl radicals, p*-nitrophenol dosimetry*

Introduction

Cavitation is the phenomenon of formation, growth, and implosion of vapor bubbles in a liquid medium. During the adiabatic collapse phase, temperature and pressure inside the cavity strongly increase and some chemical reactions involving radical species occur. For this reason, cavitation is recognized as a valid way to boost chemical and physical processes by supplying energy locally, enhancing transfer coefficients and generating oxidizing species[1]; therefore, it is currently used with different purposes in chemical engineering[1–6] and biotechnology[4] applications.

In the environmental protection field, controlled cavitation has been implemented as an Advanced Oxidation Process (AOP) for the degradation of organic nonbiodegradable pollutants in wastewaters, as it is capable to provide extremely reactive species, such as hydroxyl radicals, ·OH.[1–4,7–9] Hydrodynamic cavitation (HC) in a liquid occurs due to flow path constriction accompanied by a localized fall in the pressure. This type of cavitation has a great potential in terms of power consumption, up-scalability, simplicity of construction, and implementation in hybrid treatment solutions.[9] Contemporary research is highlighting the role of HC in waste water treatment (WWT) by focusing mainly on two fields: the effectiveness in pollutant degradation and optimization of the device configuration.[8–14] With the aim of making HC a consolidated WWT, experimental investigations have shown that it is possible to increase the treatment efficiency, particularly in hybrid solutions. Application of HC in combination with AOP is already giving some promising results in industrial applications.[14,15] In this regard, previous research works identified the critical values of operational parameters such as orifice-to-pipe ratio (β), inlet pressure (p_{in}), and cavitation number (C_v).[8,11,12]

Conversely, there is a growing interest in developing predictive codes, correlations, and theoretical models to simulate the HC physical–chemical phenomena at different levels of approximation.[1,2,8,16,17] Numerical studies, focused on the dynamics of a reactive-collapsing bubble, give the necessary physical insight for an extensive technology development: prediction of collapse pressure, temperature peaks, and concentration of chemical species. Two seminal papers published in 2000[18,19] proposed that bubble dynamics are limited by diffusion and paved the way for several studies on HC applications.[1,2,7,8,16–26] A short historical review is given in the work by Sharma et al.[21]

Notwithstanding this abundant research, HC has been only occasionally implemented for contaminated municipal and/or industrial water purification. The knowledge of the process is still limited and, to exploit the full potential of HC, it is

Correspondence concerning this article should be addressed to M. Prisciandaro at marina.prisciandaro@univaq.it.

necessary to work out mathematical models to optimize the reactor design and prove its practical feasibility as a WWT process.[1,2,7,8,11,17,21,25]

The present article offers an interpretation of the physical–chemical behavior of cavitation bubbles in a HC reactor, highlighting the existence of optimal pressure and flow rate values at a fixed geometry. The bubble dynamics model has been coupled to hydrodynamics through the constriction and the chemical reactions occurring into the collapsing bubbles over a wide range of initial bubble sizes. The cavitation event rate allows calculating an overall result comparable with the experimental values. Thus the experimental measurements of *p*-nitrophenol (pNP) degradation in a specific HC device are compared with the numerical simulations of the cavitation behavior. pNP degradation was chosen as it can be considered as an estimator of the chemical effect, more specifically of the ·OH production. The existence of an optimal pressure value has been detected both experimentally and numerically. The comparison between the two approaches contributes to a better understanding of the phenomena: modeling results offer a theoretical insight whereas the experimental evidences directly validate the model, thus allowing a step forward in effective HC reactor design.

Mathematical Model

The mathematical algorithm developed in this study is globally represented in Figure 1. It allows the simulation of single-bubble dynamic (SBD) with chemical reactions for different initial bubble sizes R_0. As visible from the sketch of the mathematical algorithm, the first output of SBD is the bubble size variation (along with inside temperature, pressure, and mass of vapor) downstream the orifice. Afterward, at the moment of collapse, the radical generation is evaluated, considering the specific bubble production, π_{OH} and the global one, Π_{OH} (by taking into account for the cavitation event rate).

The core of the algorithm is the simulation of the reactive cavitating bubble, by considering the five ordinary differential equations (ODEs) summarized in Table 1. This approach is in continuity with other research articles[16,17,20,21,26] and assumes the diffusion limited model with a boundary layer approximation introduced by Storey and Szeri[18] and Toegel et al.[19] A similar approach, which couples momentum and continuity equation, is described in a recent work[20] that reports different maps of cavitation regimes obtained by varying the operating parameters.

The main components of SBD are: (1) Rayleigh–Plesset equation for the radial motion of the bubble; (2) equation for the diffusive flux of water vapor; (3) overall energy balance treating the cavitation bubble as an open system with heat conduction through the bubble wall; (4) continuity equation; and (5) Bernoulli equation. In similarity to the aforementioned study, in the proposed modeling, gas diffusion across the bubble is ignored as its time scale is negligible as compared to bubble radial motion; fragmentation and coalescence phenomena are neglected; pressure and temperature are uniform inside the bubble and stationary in the liquid bulk and at the bubble wall; bubbles remain spherically symmetric during collapse. The integration domain $[0 \le x \le L]$ is the length of a cavitating device: a convergent–divergent nozzle, symmetric to the x axis, with a cross section A. The

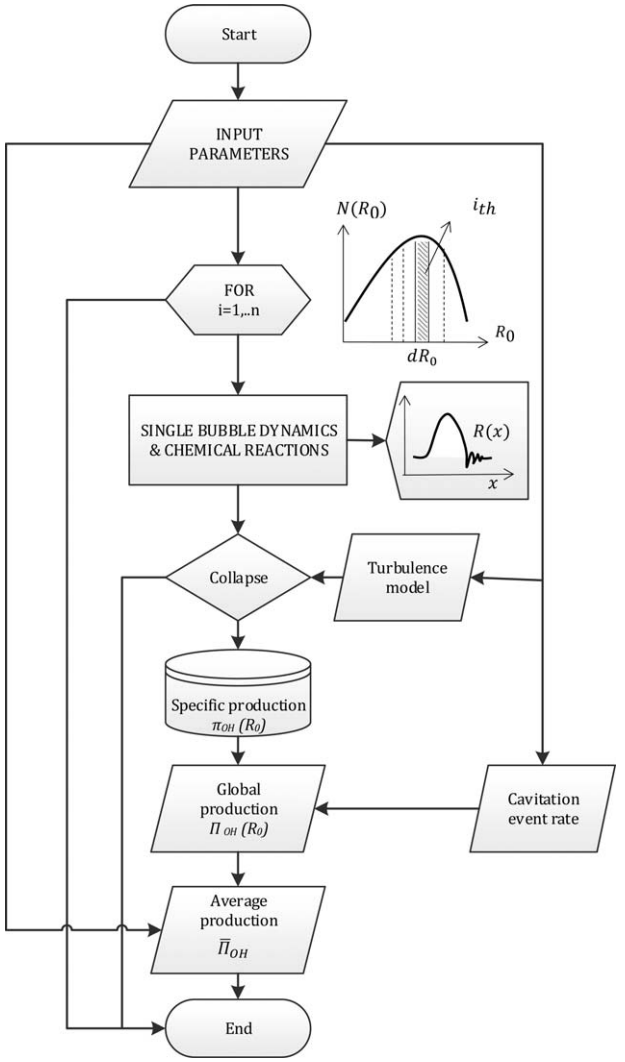

Figure 1. Sketch of the mathematical algorithm.

Table 1. Mathematical Model of SBD

Description	Equations	Initial values	#Eqs.
Rayleigh–Plesset equation	$p_l = \frac{N_{tot}\,k\,T}{4\pi(R^3-h^3)/3} - \frac{2\sigma}{R} - \frac{4\mu U}{R}\left(\frac{dR}{dx}\right) - \rho\left[R\left(U^2\frac{d^2R}{dx^2} + U\frac{dU}{dx}\frac{dR}{dx}\right) + \frac{3U^2}{2}\left(\frac{dR}{dx}\right)^2\right]$	$R(0)=R_0\frac{dR}{dx}\vert_0=0$	(1)
Mass diffusion	$u\frac{dN_w}{dx} = 4\pi R^2 D\left(\frac{C_{wR}-C_w}{l_{diff}}\right)$	$N_w(0)=0$	(2)
Energy balance	$C_{v,mix}\frac{dT}{dx} = \frac{4\pi R^2\lambda}{u}\left(\frac{T_w-T}{l_{th}}\right) - p_i\frac{dV}{dx} + (h_w-U_w)\frac{dN_w}{dx}$	$T(0)=T_w$	(3)
Continuity equation	$\left(u\frac{dA}{dx} + A\frac{du}{dx}\right)\left(1-\frac{4}{3}\pi n R^3\right) = 4\pi n\ uAR^2\frac{dR}{dx}$ where $U(x)=u+\overline{u'}\ \sin(2\pi f_T x/L)$	$U(0)=v_o$	(4)
Momentum equation	$U\frac{dU}{dx} = -\frac{1}{\rho(1-4\pi n R^3/3)}\frac{dp_l}{dx}$.	$p(0)=p_v$	(5)

model also includes the estimation of turbulent fluctuation velocity $\overline{u'}$ downstream of the orifice, following the approach first proposed by Moholkar and Pandit[16] and recently developed by Kumar et al.[20] It allows the calculation of the local velocity by adding the turbulent term to the mean flow contribution, u, derivable from the continuity equation.

The system of Eqs. 1–5 can be solved using the fourth-order/fifth-order Runge–Kutta–Fehlberg variable step-size method to obtain the variation of bubble radius, temperature, pressure, and along with the number of molecules trapped in the bubble, assuming the initial values reported in Table 1. Equation 1 can be split into two simultaneous equations by considering dR/dx as a new variable. For more details on the determination of penetration depths for mass and thermal diffusion (l_{diff}, l_{th}) and thermodynamic properties of the mixture, can be found in the work by Krishnan et al.[22]

The moment of collapse is identified according to the turbulence collapse criteria suggested by Sharma et al.,[21] based on the calculation of the fluctuation velocity. At this stage, the bubble content is modeled as a reactive mixture of compounds that cannot get out of the bubble: the radial motion of the bubble becomes extremely fast and the water vapor in the bubble cannot escape out of the gas–liquid interface, as the time scale of bubble collapse is much smaller than the time scale of diffusion and condensation.[22]

The equilibrium mole fraction of the entrapped chemical species at the peak conditions reached during the transient collapse is estimated using the Gibbs free-energy minimization technique.[27] In modeling the reactive air–vapor mixture, 16 chemical species and 45 chemical reactions have been considered; a list of reaction parameters and a detailed description of reaction rate equation is in the work by Toegel et al.[28] The solution of the chemical reaction system gives the main numerical output of specific radical production, π_{OH} (relative of a single initial nucleus of radius R_0).

As mentioned in the Introduction section and reported in Figure 1, the proposed approach introduces the calculation of a global radical production, Π_{OH}. To take into account the generation of bubbles of different sizes, the cavitation event rate J, is considered. This parameter represents the number of nuclei of a specific size that actually cavitate as a consequence of the hydraulic regime, and is evaluated following the model of Delale et al.[29] The global radical generation can be calculated by multiplying the specific contribution of a single bubble by the rate of bubble production, as in Eq. 6. Moreover, as actual experiments reflect the distribution of several bubble sizes, our calculations span the range $R_0 = 20$–250 μm, assuming a steady-state size distribution function $N(R_0)$ as suggested by Liu and Brenner.[30] In this way, the integral average reported in Eq. 7 is independent from the initial value R_0 and directly comparable with experiments, as widely suggested in the literature[7,8,13,31,32]

$$\Pi_{OH}(R_0) = J\,\pi_{OH}(R_0) \tag{6}$$

$$\overline{\Pi_{OH}} = \frac{\int \Pi_{OH}(R_0)\; N(R_0)\; dR_0}{\int N(R_0) dR_0} \tag{7}$$

Experimental Apparatus

The experimental apparatus consists of the closed loop circuit sketched in Figure 2. It incorporates a stirred reactor (with cooling system), a recycling line, a centrifugal pump, pressure and flow meters. The main branch passes through a convergent–divergent nozzle, in which cavitation occurs, and ends into the tank. The larger diameter of the Venturi reactor corresponds to the pipe diameter $d_p = 12$ mm, whereas the inner one is $d_o = 2$ mm, resulting in $\beta = 0.167$. The system is equipped with control valves V-1 and V-2 to regulate inlet pressure and consequently, the flow rate through the device.

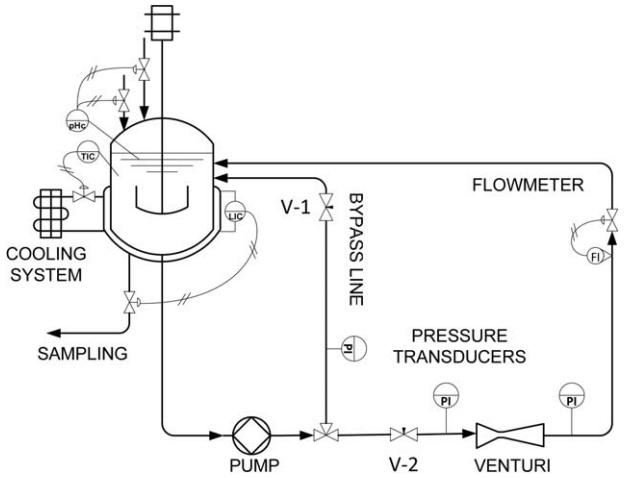

Figure 2. Schematic representation of the HC experimental setup.

The organic molecule chosen in this study is pNP (linear formula: $O_2NC_6H_4OH$, MW: 139.11 g mol^{-1}, Sigma-Aldrich in spectrophotometric grade); the pNP initial concentration was fixed at the value $pNP_0 = 0.15$ g dm^{-3} by diluting with bidistilled water. Solutions of sulphuric acid (2M) and sodium hydroxide (2M) were used to maintain the value of pH at 5. By controlling the flow through the by-pass line (3.5–6 L min^{-1}), the inlet pressure was adjusted in the range of 0.2–0.6 MPa. Samples were withdrawn from the main tank at 0–10–20–30 min and analyzed using UV-VIS spectrometry (PerkinElmer). The quantification of pNP was achieved by measuring its absorbance peaks (at 401 nm) in alkaline solution following the method proposed by Kotronarou et al.[33] Given scope of the article, only pNP conversion has been followed. Nevertheless, the method[33] includes the identification of by-products for the correction of the measured absorbance peaks.

Results and Discussion

Numerical results

In this section, the HC occurring in the experimental device is simulated following the proposed mathematical modeling (Section Mathematical Model); inlet pressure and flow rate in the Venturi varied in the ranges 0.2–0.6 MPa and 3.5–5.3 L min^{-1} m^3 s^{-1}, respectively. The integration of SBD ODE system gives the spatial prediction of the main variables downstream the constriction as represented in the sketch of mathematical algorithm (see Figure 1). This way of showing numerical results is widely used in the literature as first rough way to understand the cavitation intensity.[7,8,16,20–26] The variations of bubble radius and temperature are shown in Figure 3, for a bubble of initial radius $R_0 = 20$ μm and three values of inlet pressure $p_{in} = 0.2$, 0.4, 0.6 MPa. As visible in Figure 3, the higher the inlet pressures and flow rates the lower the bubble growth, the amount of entrapped vapor molecules and, consequently, the intensity of collapse. At higher pressures the flow rate increases,

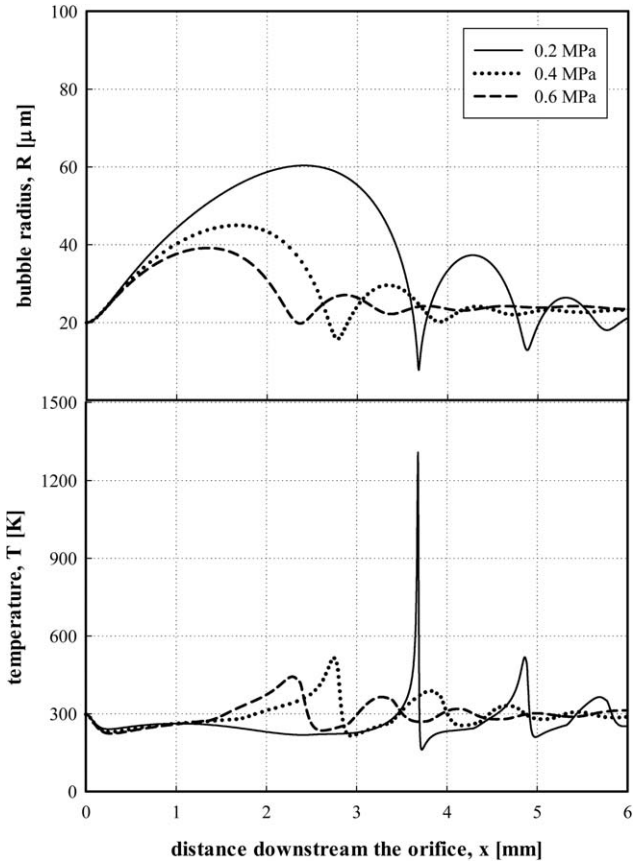

Figure 3. Single bubble dynamics simulation: Radius, *R* and temperature, *T* for an initial size of $R_0 = 20$ μm and three different level of inlet pressure, p_{in}.

leaving less time for the bubble to grow and generating higher turbulence stresses which contrast bubble expansion.[20–22] Looking at the temperature peaks, the p_{in} increase determines a lowering in the sonochemical effect, also according to the cavitation regime determined by Kumar et al.[20]

To evaluate the concentration of ·OH radicals in conjunction with the bubble collapses is a more interesting result, particularly for AOP applications. Thus, the specific radical production π_{OH} (# OH molecules/bubble) at the collapse stage, for different initial bubble sizes R_0, is represented in Figure 4. The range of initial radius R_0 chosen is 20–200 μm which covers the common experimental distributions reported in the literature.[29–35] The effect of inlet pressure is to decrease the specific production π_{OH}, this is due to the premature collapse of the bubbles occurring at higher pressures and flow rates.[21]

Figure 4 also shows a slight dependence of radical production (π_{OH}) on initial bubble size R_0. This is due to the strong dependence of the collapse bubble size on the turbulence intensity and, consequently, on inlet pressure. In other words: "no matter the initial size of the bubble," the collapse is governed by the inlet pressure at a fixed geometry. The results do not take into account the positive effect that the inlet pressure has in increasing the number of cavitating bubbles. For considering this phenomenon, the calculations have been extended to the actual nuclei production as indicated in Eq. 6. Thanks to the evaluation of the global production, it

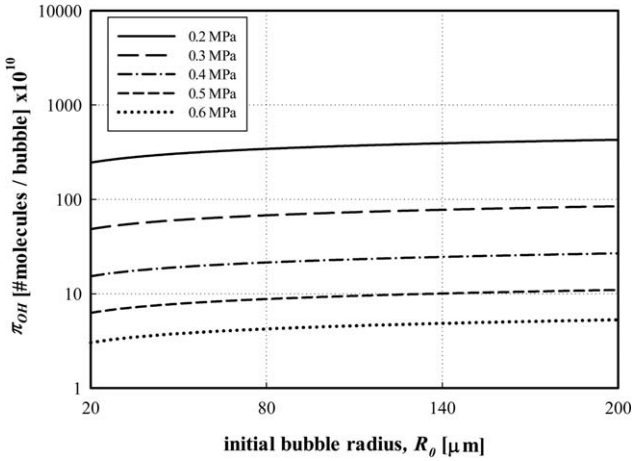

Figure 4. Specific radical production π_{OH} versus initial bubble size R_0, for five values of initial pressure in the range 0.2–0.6 MPa.

is possible to analyze the actual effect of the inlet pressure as the combination of two aspects: the increased number of cavities at higher p_{in} and the higher specific production π_{OH} at the lower ones. Figure 5 reports the values of Π_{OH} for different p_{in} levels vs. the initial bubble radius R_0. This figure is directly comparable with Figure 4; it is possible to observe that the relation between global production and pressure is not monotonic (in contrast to the one revealed for the specific production π_{OH}, which is positive and strictly monotonic). As aforementioned, this is due to higher cavitation event rate at higher inlet pressures (lower cavitation numbers).

Experimental results

To study the effect of pressure and to verify modeling results, pNP degradation tests are conducted in the Venturi reactor apparatus, varying p_{in} in the range 0.2–0.6 MPa. Figure 6 shows the pNP concentration (as a percentage of its initial value) as a function of time for different values of p_{in}. Its effect is nonmonotonic with a higher pNP conversion of 24% at 30 min and 0.45 MPa and very low chemical effect at the extreme p_{in} values (0.2 and 0.6 MPa). A useful way to

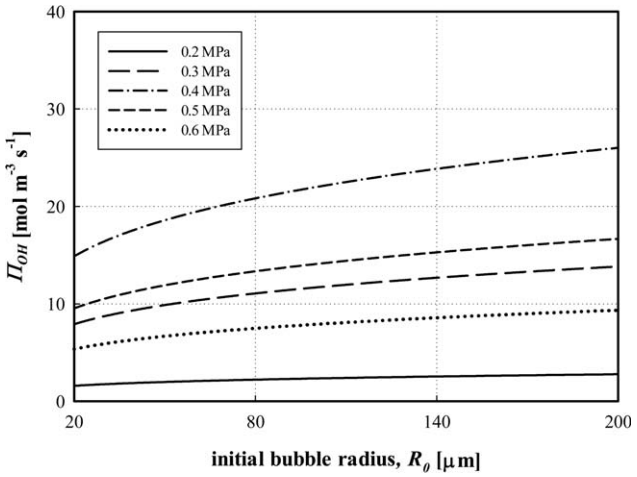

Figure 5. Global radical production π_{OH} versus initial bubble size R_0, for five values of initial pressure.

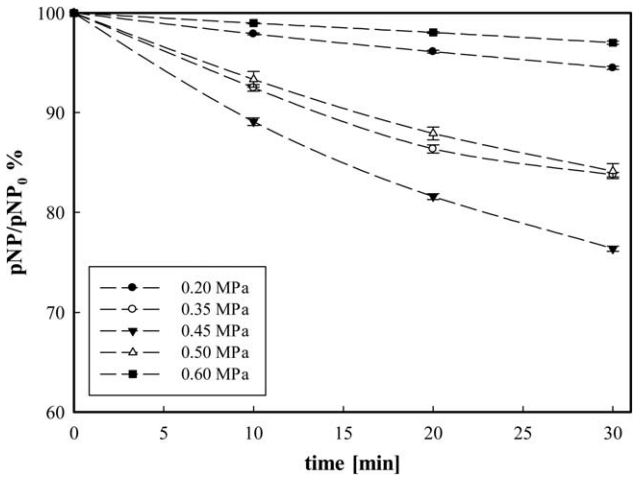

Figure 6. PNP degradation percentage versus time: inlet pressure: 0.6 MPa (■); 0.5 MPa (Δ); 0.45 MPa (▼); 0.35 MPa (○); 0.2 MPa (●).

evaluate the treatment energy efficiency is calculating the cavitational yield Y [mol J^{-1}], as in Eq. 8

$$Y(t) = \frac{\text{moles degraded per second}}{\text{power consumption}} = \frac{Q \cdot (\text{pNP}_t - \text{pNP}_0)}{Q\ \Delta P} \frac{10^3}{\text{MW}} \tag{8}$$

where Q is the flow rate and ΔP is the system pressure drop, whereas pNP_t and pNP_0 are the pNP concentration at time t and initial time, respectively.

By expressing the results in terms of cavitational yield and final removal percentage, it is possible to observe the effect of inlet pressure: Figure 7 reports the final removal percentage (after 30 min of treatment) and the cavitational yield as a function of the inlet pressure (p_{in}). Both variables increase with p_{in} until a maximum at about 0.45 MPa ($\eta \sim 24\%$ and $Y = 5.2\ 10^{-12}$ mol J^{-1}) and then decrease. This effect is consistent with other trends observed in the literature and the results previously described; Kumar et al.[36] performed a decomposition of aqueous KI solutions using HC showing the existence of a maximum chemical effect in the range of 0.4–0.5 MPa. Vichare et al.[37] recognized an optimum cavitation number for their experiments, asserting that the quantum of the total collapse pressure is the result of the single cavity features and the total number of cavities being generated (in agreement with phenomena highlighted in the previous section). Saharan et al.[38,39] reported an optimum inlet pressure of 0.5 MPa, beyond which a drop in degradation of organic dyes was observed. Similar results have been reported in the literature for the degradation of dichlorvos[36] where optimal conditions exist in the same range of pressures using orifice plate as cavitating device. An additional explanation of the maximum existence, is given by the arising of chocked cavitation. It consists of a significant increase in the number of cavities that fill the downstream area of the reactor and reduce the cavitational effects by coalescing (less collapse events) and damping energy released by the neighboring cavity collapse.[12,24,31,35,36,40] Early investigations assert that operating cavitation device near the limit of choked cavitation number, can give most effective energy utilization.[8,10,12,37–40] The critical cavitation number depends on the geometry of the system; Yan and Thorpe[40] have reported critical values for the onset of choked cavitation in a range very close to one observed in our experiments for the decrease of pNP degradation rates ($C_v < 0.25$ at $p_{in} > 0.4$ MPa).

Model validation

According to the numerical predictions reported in the previous section, a decrease in cavitation number results in a lower collapse intensity and a higher number of cavities generated. In this section, the experimental pNP degradation is discussed on the basis of the cavitation features simulated with the mathematical model. As discussed in Section Mathematical Model, the integral average $\overline{\Pi_{OH}}$ (Eq. 7) is chosen for representing the chemical effect of cavitation to be compared in ultimate analysis with experimental data.

Thus, Figure 8a reports $^{\bullet}$OH and pNP in number of moles produced/degraded per second in a cubic meter, vs. the inlet pressure p_{in}. The model results are extremely helpful in identifying the nonmonotonic dependence and comparing simulations with a measurable chemical effect (pNP degradation). The curve patterns are very similar and the maximum close to 0.4 MPa is recognized by the model which, as a consequence, is able to point out an optimal configuration. Additionally, the theoretical radical production has to be higher than the correspondent value of pNP removed (at the same abscissa, which means in the same experimental configuration) because of recombination and scavenging effects decreasing the actual radical concentration. The simulation of transport mechanisms and by-product degradation will be the next step forward in addressing the hydroxyl radical utilization. Figure 8b reports the calculations obtained for one pass through the reactor (production per cycle). The inlet fluid pressure p_{in} and the velocity at the throat are mutually dependent, this could be regarded as the most obvious reason for the higher removal increase at higher p_{in}: as pressure rises, flow rate grows, then the number of passes in the Venturi is higher. Observing that the effect of inlet pressure persists at the same number of cycles, it is possible to conclude that the enhancement of chemical activity is due to the intrinsic chemistry at different cavitation regimes, not only to the higher number of passes at higher p_{in}.

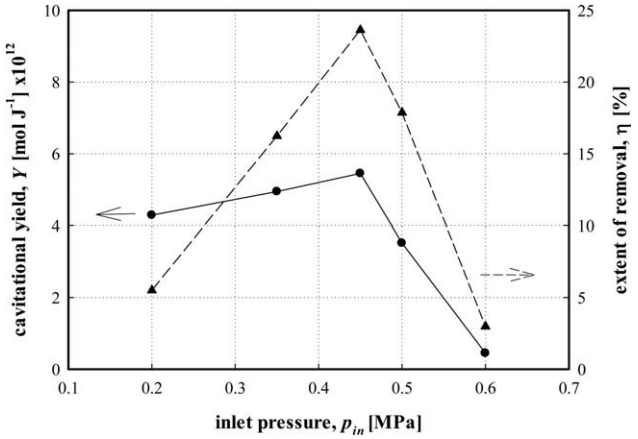

Figure 7. Effect of inlet pressure: cavitational yield (full line, ●) and final removal percentage (dashed line, ▲) vs. inlet pressure: initial concentration $C_0 = 0.15$ g dm^{-3}.

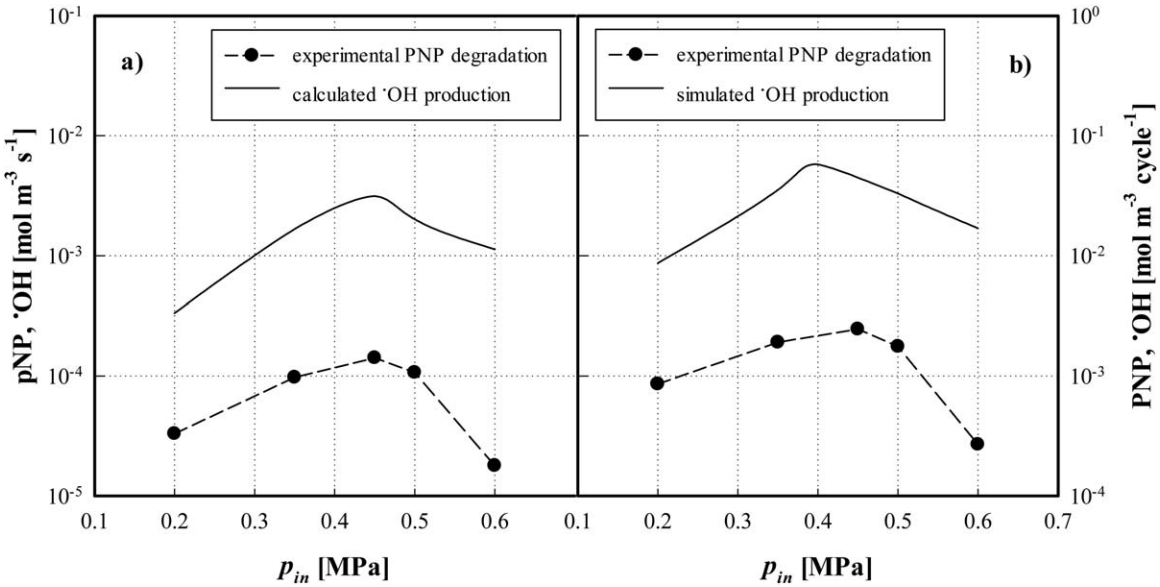

Figure 8. a-b. Experimental number of degraded pNP moles (●); numerical value of •OH moles produced (−); values related to the treatment time (a) and to one cycle into the reactor (b).

Conclusions

The simulation of a real hydrodynamic system and the integration of results upon an initial nuclei distribution can give a global quantification of the cavitational efficiency. Thanks to this approach the comparison between numerical and experimental results can be made more direct and straightforward.

In this article, a mathematical model, coupling the simulation of single reactive bubble dynamics with nucleation event rate and bubble size distribution, has been proposed. A good agreement between mathematical results and experimental observation has been found in the individuation of an optimal configuration at circa 0.45 MPa of inlet pressure (pNP removal percentage of 24% and $Y = 5.2\ 10^{-12}$ mol J^{-1}).

The proposed model can be considered a theoretical tool for optimizing geometrical and operational configuration and obtaining information and correlations for scaling-up the technology. Additionally, it can be extended to different geometries and compared with other experimental conditions to make the validation more consistent. Moreover, a next step forward could be the introduction of bubble population phenomena and the direct simulation of pollutant degradation in the mathematical algorithms: in accordance with literature, the model upgrade is individuated in the bubble interaction and in the pollutant transport mechanisms. This will be an ultimate advance for realizing comprehensive model, suitable for predicting parameter influence in different geometries and useful in reactor design and process control.

Notation

A = area of the Venturi cross section, m^2
C_v = cavitation number, dimensionless
$C_{v,mix}$ = heat capacity at constant volume of the gaseous–vapor mixture, J $kg^{-1}K^{-1}$
C_w = concentration of water molecules in the bubble, mol m^{-3}
C_{wR} = concentration of water molecules at the gas–liquid interface, mol m^{-3}
D = diffusivity, cm^2 s^{-1}
d_p = pipe inner diameter, m
d_o = diameter of the constriction, m
f_T = frequency of turbulent fluctuation, Hz
h = van der Waal's hard core radius, m
h_w = enthalpy of water molecules, J mol^{-1}
J = nucleation event rate, #bubbles m^{-3} s^{-1}
k = Boltzmann constant, m^2 kg s^{-2} K^{-1}
L = length of the cavitating device, m
l_{diff} = length scale of mass diffusion, m
l_{th} = length scale of thermal diffusion, m
MW = molar weight, g mol^{-1}
N_{tot} = total number of molecules (gas + vapor) in the bubble, mol
N_w = number of water molecules, mol
N = bubble size distribution, #bubbles m^{-1} m^{-3}
n = number density of bubbles, #bubbles m^{-3}
p_i = internal bubble pressure, Pa
p_{in} = inlet pressure, Pa
p_l = liquid total pressure, Pa
p_v = water vapour pressure, Pa
Q = flow rate, m^3 s^{-1}
R = bubble radius, m
T = bubble temperature, K
T_w = bulk liquid temperature, K
U = instantaneous velocity, m s^{-1}
$\underline{u}$ = mean velocity, m s^{-1}
$\overline{u'}$ = turbulent velocity, m s^{-1}
U_w = internal energy of water vapor molecules, J mol^{-1}
V = bubble volume, m^3
v_o = liquid velocity at *vena contracta,* m s^{-1}
x = independent variable—space, m
Y = cavitational yield, mol J^{-1}

Greek letters

β = orifice to pipe ratio, dimensionless
ΔP = pressure drop across the reactor, Pa
η = extent of removal, %
λ = thermal conductivity of bubble contents, Wm^{-2}
μ = viscosity, Pa s
Π_{OH} = global hydroxyl radical production, mol m^{-3} s^{-1}
π_{OH} = specific hydroxyl radical production, mol/bubble
ρ = water density, kg m^{-3}
σ = water surface tension, N m^{-1}

Literature Cited

1. Gogate PR, Pandit AB. Engineering design method for cavitational reactors: I. *Sonochemical reactors. AIChe J*. 2000;46:373–379.
2. Gogate PR, Pandit AB. Engineering design method for cavitational reactors: II. *Hydrodynamic cavitation. AIChe J*. 2000;46:1641–1649.

3. Gogate PR, Tatake PA, Kanthale PM, Pandit AB. Mapping of sonochemical reactors: review, analysis, and experimental verification. *AIChe J*. 2002;48:1542–1560.
4. Gogate PR, Kabadi AM. A review of applications of cavitation in biochemical engineering/biotechnology. *Biochem Eng J*. 2009;44:60–72.
5. Hamdaoui O, Naffrechoux E. An investigation of the mechanisms of ultrasonically enhanced desorption. *AIChe J*. 2007;53:363–372.
6. Tang SY, Sivakumar M. A novel and facile liquid whistle hydrodynamic cavitation reactor to produce submicron multiple emulsions. *AIChe J*. 2013;59:155–167.
7. Capocelli M, Joyce E, Lancia A, Mason TJ, Musmarra D, Prisciandaro M. Sonochemical degradation of estradiols: incidence of ultrasonic frequency. *Chem Eng J*. 2012;210:9–17.
8. Capocelli M, Prisciandaro M, Musmarra D, Lancia A. Understanding the physics of advanced oxidation in a venturi reactor. *Chem Eng Trans*. 2013;32:691–696.
9. Chakinala AG, Gogate PR, Chand R, Bremner DH, Molina R, Burgess AE. Intensification of oxidation capacity using chloroalkanes as additives in hydrodynamic and acoustic cavitation reactors. *Ultrason Sonochem*. 2008;15:164–170.
10. Saharan VK, Rizwani M, Malani A, Pandit AB. Effect of geometry of hydrodynamically cavitating device on degradation of orange-G. *Ultrason Sonochem*. 2013;20:345–353.
11. Braeutigam P, Franke M, Wu, Z-L, Ondruschka B. Role of different parameters in the optimization of hydrodynamic cavitation. *Chem Eng Technol*. 2010;33:932–940.
12. Joshi RK, Gogate PR, Degradation of dichlorvos using hydrodynamic cavitation based treatment strategies. *Ultrason Sonochem*. 2012;19:532–539.
13. Amin LP, Gogate PR, Burgess AE, Bremner DH. Optimization of a hydrodynamic cavitation reactor using salicylic acid dosimetry. *Chem Eng J*. 2010;156:165–169.
14. Chakinala AG, Bremner DH, Namkung K, Burgess AE, Multivariate analysis of phenol mineralization by combined hydrodynamic cavitation and heterogeneous advanced Fenton processing. *Appl Catal B-Environ*. 2008;78;11–18.
15. Chakinala AG, Gogate PR, Burgess AE, Bremner DH, Industrial wastewater treatment using hydrodynamic cavitation and heterogeneous advanced Fenton processing. *Chem Eng J*. 2009;152:498–502.
16. Moholkar VS, Pandit AB. Bubble behavior in hydrodynamic cavitation: effect of turbulence. *AIChE J*. 1997;43:164–1648.
17. Capocelli M, Prisciandaro M, Lancia A, Musmarra D. Modeling of cavitation as an advanced wastewater treatment. *Desalin Water Treat*. 2013;51:1609–1614.
18. Storey BD, Szeri J. Water vapour, sonoluminescence and sonochemistry. *Proc R Soc A Math Phys Eng Sci*. 2000;456:1685–1709.
19. Toegel R, Gompf B, Pecha R, Lohse D. Does water vapor prevent upscaling sonoluminescence? *Phys Rev Lett*. 2000;85:3165–3168.
20. Kumar P, Khanna S, Moholkar V. Flow regime maps and optimization thereby of hydrodynamic cavitation reactors. *AIChE J*. 2012; 58(12):3858–3866.
21. Sharma A, Gogate P, Mahulkar A, Pandit A. Modeling of hydrodynamic cavitation reactors based on orifice plates considering hydrodynamics and chemical reactions occurring in bubble. *Chem Eng J*. 2008;143:201–209.
22. Krishnan JS, Dwivedi P, Moholkar VS. Numerical investigation into the chemistry induced by hydrodynamic cavitation. *Ind Eng Chem Res*. 2006;45:1493–1504.
23. Chakma S, Moholkar VS. Physical mechanism of sono-fenton process. *AIChe J*. 2013;59:4303–4313.
24. Sivasankar T, Moholkar VS. Mechanistic approach to enhancement of the yield of a sonochemical reaction. *AIChe J*. 2007;53:1132–1143.
25. Ozonek J. *Application of Hydrodynamic Cavitation in Environmental Engineering*. London: CRC Press, 2012.
26. Mishra SK, Deymier P, Muralidharan K, Frantziskonis G, Pannala S, Simunovic S. Modeling the coupling of reaction kinetics and hydrodynamics in a collapsing cavity. *Ultrason Sonochem*. 2010;17:258–265.
27. Barba D, Prisciandaro M, Salladini A, Mazziotti di Celso G. The Gibbs free energy gradient method for RDF gasification modelling. *Fuel*. 2011;90:1402–1407.
28. Toegel R, Hilgenfeldt S, Lohse D. Suppressing dissociation in sonoluminescing bubbles: the effect of excluded volume. *Phys Rev Lett*. 2002;88:3–6.
29. Delale CF, Okita K, Matsumoto Y. Steady-state cavitating nozzle flows with nucleation. *J Fluids Eng*. 2005;127:770–777.
30. Liu Z, Brenner CE. Models of cavitation event rate. In: Proceedings of CAV95 International Symposium of Cavitation, Deauville, France, 1995:321–328.
31. Wang Y, Brenner C. One-dimensional bubbly cavitating flows through a converging-diverging nozzle. *Trans ASME*. 1998;120:166–170.
32. Colussi AJ, Weavers LK, Hoffmann MR. Chemical bubble dynamics and quantitative sonochemistry. *J Phys Chem A*. 1998;102:6927–6934.
33. Kotronarou A, Mills G, Hoffmann MR. Ultrasonic irradiation of p-nitrophenol in aqueous solution. *J Phys Chem*. 1991;95:3630–3638.
34. Liu Z, Sato K, Brennen C. Cavitation nuclei population dynamics in a water tunnel. *ASME*. 1993;153:119–125.
35. Delale CF, Schnerr GH, Sauer J. Quasi-one-dimensional steady-state cavitating nozzle flows. *J Fluid Mech*. 2001;427:167–204.
36. Kumar PS, Kumar MS, Pandit A. Experimental quantification of chemical effects of hydrodynamic cavitation. *Chem Eng Sci*. 2000; 55:1633–1639.
37. Vichare NP, Gogate PR, Pandit AB. Optimization of hydrodynamic cavitation using a model reaction. *Chem Eng Technol*. 2000;23:683–690.
38. Saharan VK, Badve MP, Pandit AB. Degradation of reactive red 120 dye using hydrodynamic cavitation. *Chem Eng J*. 2011;178: 100–107.
39. Saharan VK, Pandit AB, Satish Kumar PS, Anandan S. Hydrodynamic cavitation as an advanced oxidation technique for the degradation of acid red 88 dye. *Ind Eng Chem Res*. 2012;51:1981–1989.
40. Yan Y, Thorpe RB. Flow regime transitions due to cavitation in the flow through an orifice. *Int J Multiphase Flow*. 1990;16:1023–1045.

Manuscript received Jan. 20, 2014, and revision received Mar. 11, 2014.